Journal of Biomechanics 85 (2019) 59–66

Contents lists available at ScienceDirect

Journal of Biomechanics

journal homepage: www.elsevier.com/locate/jbiomech
www.JBiomech.com

Influence of loading condition and anatomical location on human cortical bone linear micro-cracks

Rémy Gauthier [a,b], Max Langer [b], Hélène Follet [c], Cécile Olivier [b,d], Pierre-Jean Gouttenoire [b,d], Lukas Helfen [d,f], Frédéric Rongiéras [a,e], David Mitton [a], Françoise Peyrin [b,d,*]

[a] Univ Lyon, Université Claude Bernard Lyon 1, IFSTTAR, LBMC UMR_T9406, F69622 Lyon, France
[b] Univ Lyon, CNRS UMR 5220, Inserm U1206, INSA Lyon, Université Claude Bernard Lyon 1, Creatis, F69621 Villeurbanne Cedex, France
[c] Univ Lyon, Université Claude Bernard Lyon 1, INSERM, LYOS UMR1033, F69008 Lyon, France
[d] European Synchrotron Radiation Facility, CS 40220, 38043 Grenoble Cedex 9, France
[e] Service Chirurgie Orthopédique et Traumatologie - Hôpital Desgenettes, 69003 Lyon, France
[f] Institute for Photon Science and Synchrotron Radiation, Karlsruhe Institute of Technology (KIT), D-76131 Karlsruhe, Germany

ARTICLE INFO

Article history:
Accepted 3 January 2019

Keywords:
Human cortical bone
Inter-site
Strain rate
Micro-cracks
Synchrotron radiation
Computed tomography

ABSTRACT

Human cortical bone fracture toughness depends on the anatomical locations under quasi-static loading. Recent results also showed that under fall-like loading, cortical bone fracture toughness is similar at different anatomical locations in the same donor. While cortical bone toughening mechanisms are known to be dependent on the tissue architecture under quasi-static loading, the fracture mechanisms during a fall are less studied. In the current study, the structural parameters of eight paired femoral diaphyses, femoral necks and radial diaphyses were mechanically tested under quasi-static and fall-like loading conditions (female donors, 70 ± 14 y.o., [50–91 y.o.]). Synchrotron radiation micro-CT imaging was used to quantify the amount of micro-cracks formed during loading. The volume fraction of these micro-cracks was significantly higher within the specimens loaded under a quasi-static condition than under a loading representative of a fall. Under fall-like loading, there was no difference in crack volume fraction between the different paired anatomical locations. This result shows that the micro-cracking toughening mechanism depends both on the anatomical location and on the loading condition.

1. Introduction

The study of bone fracture is a complex problem requiring investigation of bone architectural properties at different length scales (Seeman and Delmas, 2006). Several crack propagation mechanisms in human cortical bone have been demonstrated in the past, such as crack bridging (Nalla et al., 2004), fibrillar sliding (Gupta et al., 2013) and micro-damage (Diab and Vashishth, 2005; Nalla et al., 2004; Vashishth et al., 1997; Zioupos et al., 2008).

There are two main distinct forms of micro-damage: diffuse damages and linear micro-cracks that can be distinguished by their surface to volume ratio (Tang and Vashishth, 2010; Vashishth, 2007). Diffuse damages appear as a bundle of submicroscopic cracks that mainly diffuse in the organic phase of the collagen matrix (Poundarik et al., 2012; Vashishth et al., 2000). Linear micro-cracks are planar defects that mostly spread in the longitudinal direction, parallel to the osteonal canals in cortical bone (Mohsin et al., 2006). Both of these damages are known to have an influence on bone ultimate properties (Danova et al., 2003; Diab and Vashishth, 2005; Turnbull et al., 2014). It has been shown that, wether bone is more able to undergo diffuse damages formation or micro-cracking is dependent on the age of the subject. A younger subject will undergo more diffuse damages formation whereas an older one will undergo more micro-cracking (Diab et al., 2006). The population of donors used in the current study is 70 y.o. in average (cf. 2.1). This is why the following is focused on linear micro-cracks.

Various studies have evidenced that micro-cracks significantly accumulate during a critical loading (Follet et al., 2011; Norman and Wang, 1997; Schaffler et al., 1995). Micro-damage can relax the material by consuming the energy to create the surface of the newly formed micro-crack (Griffith, 1921) during their formation resulting in the slowdown of the main crack propagation (Nalla et al., 2004; Ritchie, 1999, 1988; Zioupos et al., 2008). The effect of strain rate on the micro-cracks has nevertheless rarely

* Corresponding author at: Univ Lyon, CNRS UMR 5220, Inserm U1206, INSA Lyon, Université Claude Bernard Lyon 1, Creatis, F69621 Villeurbanne Cedex, France.
E-mail address: peyrin@esrf.fr (F. Peyrin).

https://doi.org/10.1016/j.jbiomech.2019.01.008
0021-9290/

been studied. Whereas a significant decrease of bone fracture toughness, the energy needed to initiate and propagate a crack through bone microstructure, has been recorded when increasing the loading rate (Gauthier et al., 2017; Kulin et al., 2011; Ural et al., 2011; Zimmermann et al., 2014). Zioupos et al. showed that in 2D there are less micro-cracks at higher loading rates (Zioupos et al., 2008).

The other role of micro-cracks during life is their interaction with the osteocyte system, which forms a dense network within bone tissue. Osteocytes are included in ellipsoidal lacunae (Marotti, 1979) and communicate through numerous small channels called canaliculi (Bonewald, 2011). It is assumed that micro-cracks can be sensed by the osteocyte lacunae. When a micro-crack opens onto an osteocyte lacuna or canaliculus, the osteocytes appear to use the Wnt/β-catenin pathway to transmit signals of mechanical loading to cells on the bone surface (Bonewald and Johnson, 2008) and thus initiate the remodeling process (Burr et al., 1985). This is why the investigation of these micro-cracks is of great interest.

While cracks propagate within the 3D bone structure, only a few observation techniques are available to quantify their morphology in 3D (Poundarik and Vashishth, 2015). The first observation of micro cracks in 3D were obtained with microscopic imaging after serial sectioning (Mohsin et al., 2006) or confocal microscopy (Zarrinkalam et al., 2005). Conventional micro computed tomography (μCT) (Steiner et al., 2016; Tang et al., 2007; Tang and Vashishth, 2007; Turnbull et al., 2014; Wang et al., 2007), generally associated to a contrast agent has been used to detect damaged zones but its resolution is not sufficient to image directly micro cracks. 3D Synchrotron Radiation μCT (SR-μCT) (Gauthier et al., 2018b; Katsamenis et al., 2013; Larrue et al., 2011; Voide et al., 2009; Wolfram et al., 2016) has been used to image and quantify micro-cracks. This later technique is non-destructive and permits to reach a sufficiently high spatial resolution (below the micrometer) to capture micro-cracks even at its smallest dimension.

In previous studies, the assessment of micro-cracks was performed at only one anatomical location, the femoral diaphysis. We showed that cortical bone fracture toughness and structural properties depend on the anatomical location (Gauthier et al., 2018a, 2018b, 2017). Human cortical bone fracture properties in other sites where *in vivo* fracture may occur, such as the radius or the femoral neck, should be considered (Court-Brown and Caesar, 2006). Therefore, in this study we investigate the influence of critical mechanical loading on 3D micro-crack morphology in human cortical bone from different paired anatomical locations at two different loading rates. The aim is to provide new insights in the micro-cracking toughening mechanism that is known to be a major determinant for crack propagation mechanisms.

The focus of the current study is thus to analyze potential differences between the 3D micro-cracks properties on paired femoral diaphyses, femoral necks and radial diaphyses considering quasi-static and fall representative loading conditions.

2. Materials and methods

2.1. Sample preparation and imaging

The sample preparation in the current study was previously described in detail (Gauthier et al., 2018b). A brief summary and some additional information are given below.

Two contiguous cortical bone rectangular samples were extracted from eight paired femoral diaphyses, femoral necks and radial diaphyses that were collected from eight female subjects (70 ± 14 y.o., [50–91 y.o.], French Ministry of Education and Research, authorization no. DC-2015-2357). The eight donors of the current study are a sub-population of the donors used in (Gauthier et al., 2017). No additional information regarding disease status or medication history was available. The samples were prepared following the ASTM E-1820 for Single Edge Notched Bending (SENB) fracture toughness experiments (Gauthier et al., 2017; The American Society of Mechanical Engineers (ASME), (2006)). The final dimensions of the samples were W = 2.1 ± 0.1 mm in width, B = 1.0 ± 0.1 mm in thickness and between 20 and 25 mm in length. A notch was cut in the middle of each sample, perpendicularly to the long surface, on the wide side. The samples were subjected to a SENB fracture toughness test until fracture (Fig. 1, (Gauthier et al., 2017)). Two contiguous samples per donor were machined. One of the samples was loaded quasi-statically, with a strain representative of walking ($10^{-4}\,s^{-1}$), while the other was loaded with a strain rate representative of a fall ($10^{-1}\,s^{-1}$, (Foldhazy, 2005)). The values of the fracture toughness parameters obtained are given in the supplementary materials (Table S1). After being loaded, samples were broken in two parts. One of the resulting sample pieces was imaged using SR-μCT, resulting in an imaged population of 48 samples (8 donors × 3 sites × 2 strain rates). On each sample, two volumes of interest (VOI) were imaged. The VOI number 1 (VOI1, Fig. 1) was chosen outside of the support rollers used for the mechanical test. Since there was no particular mechanical stress applied there, VOI1 was considered as a control and corresponds to the region analyzed in a previous study (Gauthier et al., 2018b). The second VOI (VOI2, Fig. 1) contains the fracture surface and the surrounding damaged region, where the main crack has propagated during the mechanical test, therefore having been subjected to a high stress concentration state. Before imaging, samples followed a delipidation protocol one week before imaging: the samples were immerged in acetone for 30 min, then rinsed with water, and finally dehydrated by successive immersion in 70% and nearly 100% ethanol baths for a maximum period of two days.

All samples were imaged by SR-μCT performed on beamline ID19 at the ESRF (European Synchrotron Radiation Facility, Grenoble, France). For each sample, 2000 projection images were recorded over a total rotation of 360°, with a counting time of 0.3 s per projection and a total scan time of 14 min. Both phase and absorption CT images were obtained with a voxel size of 0.7 μm^3. The phase retrieval was performed using Paganin's algorithm (Paganin et al., 2002), with the parameter δ/β set at 572 (Gauthier et al., 2018b). Finally, volumes of 2048^3 voxels were obtained. A total of 96 absorption and phase 3D images were obtained, yielding a total data set of 6.1 Tb. The imaged VOIs were cropped in order to reduce the processing time. The analyzed volume size was 1 mm × 0.5 mm × 0.5 mm. For the VOIs containing the fracture surface, the cropped volumes start at the initial notch tip and follow the main crack over 500 μm, where the main crack propagation mechanisms occur (Koester et al., 2008) (Fig. 2).

2.2. Image analysis

2.2.1. Micro-cracks segmentation

First, a mask of the bone was extracted by thresholding using Otsu's method followed by a median filter to fill in osteocyte lacunae and other small porosities. A mask of the Haversian canals was then generated as the complement of the bone mask. Osteocyte lacunae and micro-cracks were then segmented using hysteresis thresholding with a low and a high value for the threshold. The low value of the threshold is used to select the voxels within the osteocyte lacunae whereas the higher one refines the segmentation by selecting the connected voxels with a higher intensity.

Identification of osteocyte lacunae and micro-cracks was done based on geometric parameters. This method has already been used in previous studies (Dong et al., 2014; Gauthier et al.,

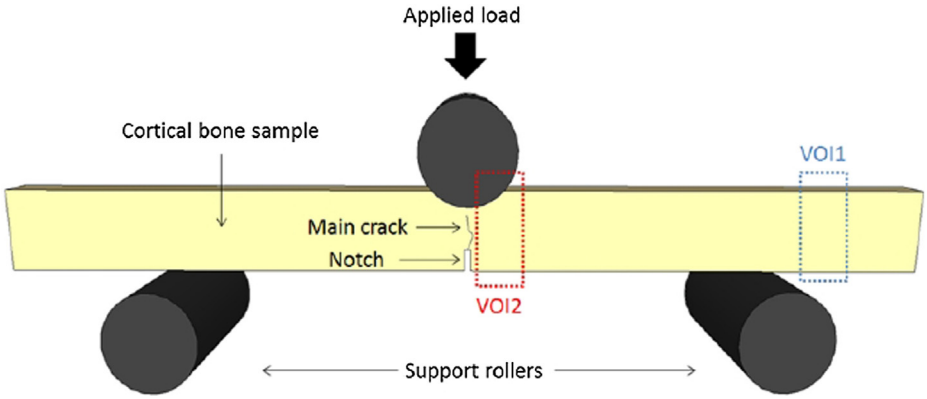

Fig. 1. Schematic of the mechanical apparatus, and illustration of the two VOIs.

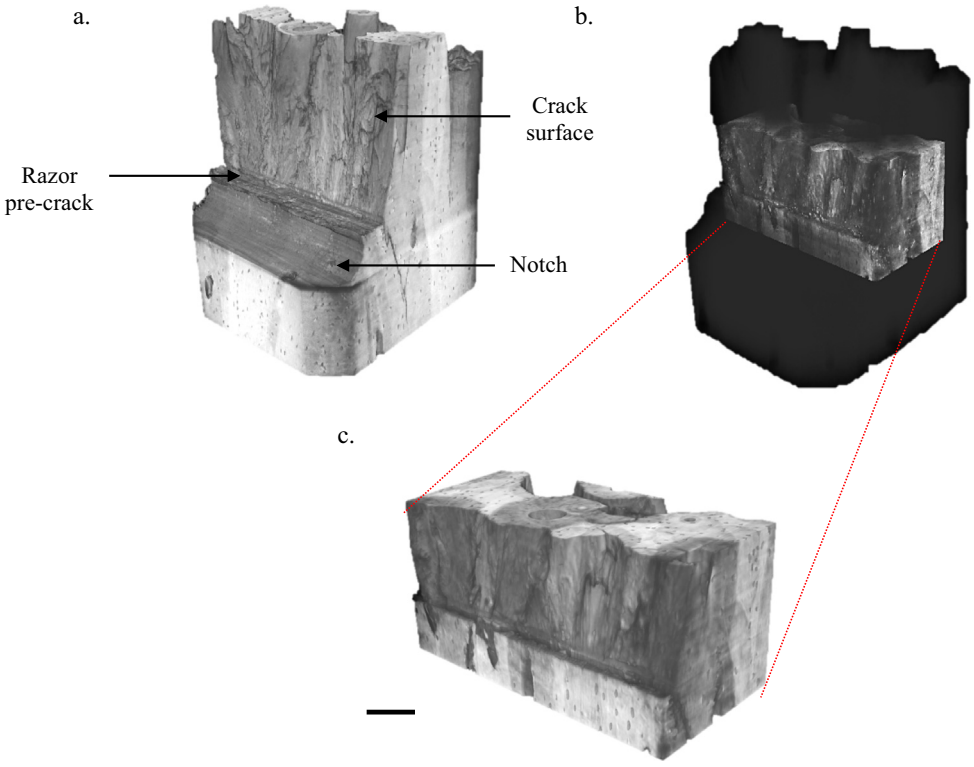

Fig. 2. 3D Volume rendering of human radial diaphysis sample tested under quasi-static loading conditions: a. is the complete reconstructed cracked VOI; b. is the superposition of the complete and cropped VOI; c. is the rendering of the cropped VOI. Scale bar = 200 μm.

2018b; Larrue et al., 2011). For this purpose, the porosities were fitted with ellipsoids. Subsequently, different morphometric parameters were used to identify whether porosity is an osteocyte lacuna or a micro-cracks (using micro-cracks, μCr, as an example), namely:

- Object volume (μCr.V), obtained as the number of voxels inside the object multiplying by the volume of one voxel.
- The three axes sizes of the fitted ellipsoid ($\mu Cr.L_1/\mu Cr.L_2/\mu Cr.L_3$) (Larrue et al., 2011).
- Object thickness (μCr.Th), considered as the diameter of the maximal fitting sphere within the object (Martín-Badosa et al., 2003).
- The object Structural Model Index (μCr.SMI), calculated as in (Schladitz et al., 2006).

Table 1
Summaries of inclusion criteria for the segmentation of micro-cracks and secondary cracks.

Inclusion criteria	
Micro-cracks	Secondary cracks
$\mu CrV > 500\ \mu m^3$	$2dCr.V > 500\ \mu m^3$
$\mu Cr.L1/\mu Cr.Th > 15$ and $\mu Cr.L2/\mu Cr.Th > 8$	$2dCr.L1/2dCr.Th > 35$, $2dCr.L2/2dCr.Th > 35$ and $2dCr.L3/2dCr.Th > 20$
$\mu Cr.L_1/\mu Cr.L_3 < 5$ and $\mu CrL_2/\mu Cr.L_3 < 3$	$2dCr.SMI < 2.5$
$\mu Cr.SMI < 2.5$	–

The objects that satisfy the criteria given in Table 1 were considered micro-cracks following (Dong et al., 2014) and (Gauthier et al., 2018b).

By qualitatively assessing VOI1, we observed another type of crack, different from the micro-cracks discussed above, but also due to external loading. These cracks, which we call secondary cracks (2ndCr), appear to be much larger than what we labelled as micro-cracks above. They are larger than the small micro-cracks, resulting in a shape that depends on the crossed microstructure. They present a high value of L1, L2 and also L3, at the opposite of the micro-cracks that have low L3, which is close to the thickness defined by the sphere method (Fig. 3). The criteria we used were: 2ndμCr.L1/2ndμCr.Th > 35; 2ndμCr.L2/2ndμCr.Th > 35 and 2ndμCr.L3/2ndμCr.Th > 20, and these criterions have been determined empirically. A summary of these criteria is given in Table 1.

2.2.2. Analysis of micro-cracks

The different geometric parameters listed above were analyzed for the three different features (i.e. lacunae, micro-cracks and secondary cracks). The dimensions of the micro-cracks were taken as the three axes of the best fitting ellipsoid, μCr.L1 (μm), μCr.L2 (μm) and μCr.L3 (μm). The mean individual volume and surface, μCr.V (μm^3) and μCr.S (μm^2) were evaluated by following the intrinsic volume method (Dong et al., 2014; Schladitz et al., 2006).

We calculated the micro-crack, secondary crack and total crack volume fraction, respectively denoted μCr.V/BV (%), 2dCr.V/BV (%) and TotCr.V/BV (%), defined as the sum of the two previous ones. Here, BV is the Bone Volume that represents the bone tissue and not the total volume (TV) that is the addition of both bone and Haversian canals volumes (Gauthier et al., 2018b).

The authors choose to measure the crack volume fraction as the ratio between the crack volume (μCr.V) and the bone volume (BV) and not the total volume (TV) to avoid considering the difference of porosity between the locations for the calculation of the parameter (Gauthier et al., 2018b). Furthermore, micro-cracks appear within the bone tissue, this makes it more relevant to express their volume fraction with respect to BV.

The values obtained for the control group are given in (Gauthier et al., 2018b).

2.3. Statistical analysis

In order to analyze the influence of the anatomical location on the one hand, and to investigate the influence of loading condition in on the other hand, we used Friedman test for independent samples before applying a Wilcoxon test for paired samples using StatView (Abaqus, USA) to analyze differences between the different groups. Paired analyses were performed both for the group of samples harvested from a same bone but subjected to different loading conditions, and for the group of samples subjected to the same loading condition but harvested from different paired anatomical locations on a same donor. Results with p-value <0.05 were considered as significant.

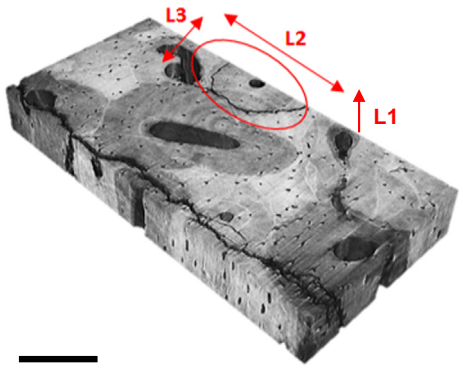

Fig. 3. Volume rendering of radial diaphysis cortical bone samples loaded under quasi-static conditions. Note the secondary crack surrounding the osteon. The best fitting ellipsoid for this crack has high dimensions in the three directions. The L1 dimension is the larger one and is along the osteon. The L3 dimension is large because of the deviation of the secondary crack. Scale bar = 200 μm.

3. Results

Figs. S1–S3 in the supplementary materials show 3D renderings of samples loaded under quasi-static and fall-like loading conditions from the femoral diaphysis, the femoral neck and radial diaphysis, respectively. Table S1 in the supplementary materials gives the individual values for each donor and for each anatomical location of the linear toughness (K_{Ic}), non linear toughness (K_{Jc}), osteonal canals volume fraction (Ca.V/TV) and osteocytes lacunae volume fraction (Lc.V/BV). These parameters have been measured in previous studies (Gauthier et al., 2018b, 2017).

3.1. Influence of mechanical loading

The effect of mechanical loading on micro-crack volume fraction (μCr.V/BV and TotCr.V/BV) is reported in Table 2. The results are expressed as the ratio between the averaged of the cracked group and that of the control group. Both under quasi-static and fall-like loading conditions, μCr.V/BV and TotCr.V/BV were significantly higher compared to the control state for femoral diaphysis, femoral neck and radial diaphysis.

3.2. Influence of strain rate

Fig. 4 shows the bar chart of TotCr.V/BV for the three studied locations, and for the control and cracked VOIs, up to three fold for quasi-static between radius and femoral neck. Descriptive statistics of the measured morphometric parameters are reported in Table 3. We observe that there are significant differences in the morphology of the micro-cracks at different locations under quasi-static loading. These differences are less pronounced under fall-like loading.

3.3. Influence of anatomical site

Considering the quasi-static loading conditions, micro-cracks observed in the radius have a larger median individual surface (μCr.S) than in the femoral diaphysis and femoral neck, by 42% and 48% respectively. The individual crack volume (μCr.V) is only larger (by 53%) in the femoral neck.

Concerning secondary cracks, in the radius, these cracks have a larger third axis than in the femoral diaphysis (27% higher) and the femoral neck (28% higher).

Table 2
Ratio between control and cracked VOIs for quasi-static and fall-like loading condition. The results are consider as significant when the difference between the loaded and the control samples is significant.

Micro-cracks parameters	Femoral diaphysis	Femoral neck	Radial diaphysis
	Quasi-static		
μCr.V/BV	5.03*	2.37*	10.22*
TotCr.V/BV	21.01*	8.63*	25.72*
	Fall		
μCr.V/BV	2.36*	2.98*	3.09*
TotCr.V/BV	8.07*	5.72*	5.99*

* $p < 0.05$, ns non-significant.

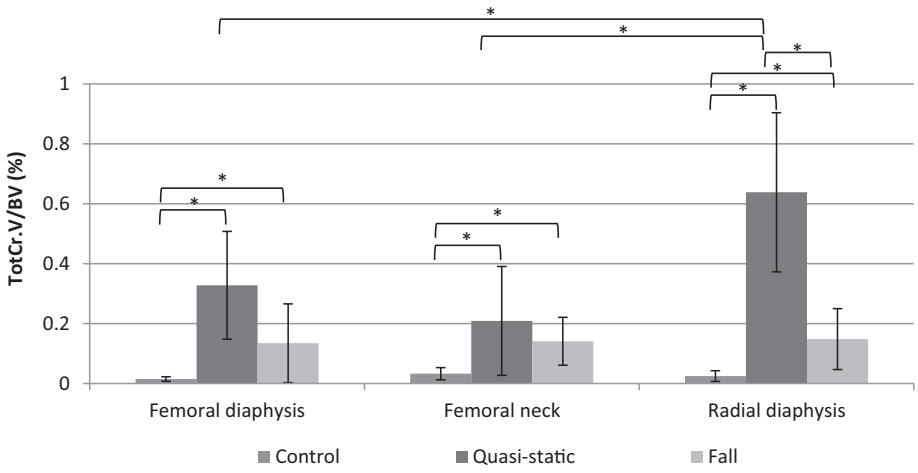

Fig. 4. Bar charts of TotCr.V/BV values in % for the three anatomical locations (* p-value <0.05).

Table 3
Geometrical parameters: mean (interquartile range) on control and cracked VOIs loaded under quasi-static and fall-like conditions. Values for the secondary cracks are not given for the control group because there were not such structural features in these VOIs.

Micro-cracks parameters	Loading rate	Femoral diaphysis	Femoral neck	Radial diaphysis
μCr.L_1 (μm)	Control	72.94 (39.29)	67.12 (21.50)	69.69 (50.45)
	Quasi-static	77.12 (22.74)	78.24 (18.41)	80.88 (14.66)
	Fall	78.45 (12.62)	85.19 (6.01)	75.91 (23.43)
μCr.L_2 (μm)	Control	28.61 (12.70)	30.04 (10.01)	30.91 (14.50)
	Quasi-static	35.82 (10.03)	34.81 (22.88)^{r*}	41.85 (4.72)^{n*}
	Fall	34.18 (5.26)	27.74 (6.75)^{r*}	35.56 (11.30)^{n*}
μCr.Th (μm)	Control	1.92 (0.20)	1.99 (0.31)	2.06 (0.21)
	Quasi-static	1.98 (0.13)	1.92 (0.07)^{r*}	2.13 (0.18)^{n*}
	Fall	2.05 (0.26)	2.01 (0.27)	2.18 (0.20)
μCr.S (10^3 μm^2)	Control	3.18 (3.14)	4.45 (3.63)	5.18 (7.35)
	Quasi-static	5.02 (3.32)^{r*}	4.95 (1.26)^{r*}	10.14 (4.77)$^{d*\ n*}$
	Fall	5.13 (1.45)	6.86 (4.05)	6.29 (3.95)
μCr.V (10^3 μm^3)	Control	2.26 (2.20)	3.74 (2.89)	4.29 (6.24)
	Quasi-static	4.08 (2.94)^{r*}	3.74 (1.18)^{r*}	9.06 (6.63)d$^{*\ n*}$
	Fall	4.52 (1.34)	5.70 (3.49)	5.44 (4.37)
μCr.V/BV (% × 10^3)	Control	16.47 (9.49)	23.61 (19.39)	24.32 (17.66)
	Quasi-static	82.82 (39.85)^{r*}	56.00 (39.02)^{r*}	248.53 (156.61)$^{d*\ n*}$
	Fall	38.86 (17.47)^{n*r*}	70.45 (20.23)^{d*}	75.16 (29.13)^{d*}
	Relative difference (%)	ns	ns	−70*
2dCr.L3 (μm)	Quasi-static	74.51 (33.01)^{r*}	74.49 (19.622)^{r*}	100.91 (25.73)$^{d*\ n*}$
	Fall	81.29 (25.83)	65.77 (35.65)	69.68 (18.74)
2ndCr.S (10^3 μm^2)	Quasi-static	135.53 (127.12)	150.06 (83.29)	231.13 (91.02)
	Fall	132.72 (94.75)	152.83 (136.36)	181.64 (88.90)
2ndCr.V (10^3 μm^3)	Quasi-static	133.36 (110.15)	147.22 (60.24)	221.72 (90.35)
	Fall	130.03 (95.66)	138.92 (127.76)	146.05 (79.33)
TotCr.V/BV (% × 10^3)	Quasi-static	345.87 (177.81)^{r*}	203.76 (176.40)^{r*}	625.63 (260.15)$^{d*\ n*}$
	Fall	132.84 (128.29)	118.14 (84.68)	125.69 (84.68)
	Relative difference (%)	ns	ns	−80*

^{d}Different from femoral diaphysis, ^{n}different from femoral neck, ^{r}different from radial diaphysis.
*p < 0.05, ns: Non-Significant.
Relative difference are given between the quasi-static and the fall-like loading conditions.

Regarding micro-crack volume fraction (μCr.V/BV), a significant difference was only measured in the radius, where the volume fraction was higher by 48% under quasi-static loading. The same result is observed when considering the total volume fraction of cracks formed within the tissue. A significant difference was observed for the radius, with a TotCr.V/BV higher for the radius by 78%, under a quasi-static condition.

4. Discussion

Bone fragility is a complex issue that needs to be better understood in order to better to predict and prevent fracture, particularly in the elderly. Bone fracture toughness depends on anatomical location (Gauthier et al., 2018a, 2017) and more specifically on the tissue micro-structure at different length-scales (Graham

et al., 2013; Granke et al., 2016). The hierarchical bone organization is associated to different toughening mechanisms that can slow down crack propagation. In the current study, we focused on the formation of micro-cracks within cortical bone considering different paired anatomical locations and two loading conditions.

Most of the previous studies characterizing micro-cracks considered fatigue tests that involve different mechanisms than the fracture toughness tests performed here (Haupert et al., 2015; Mohsin et al., 2006; O'Brien et al., 2000). Wolfram et al. performed tensile mechanical experiments on dumbbell-shaped human cortical bone samples from femoral diaphysis loaded in either tension, compression, or torsion (Wolfram et al., 2016). The mechanical loading was not sustained until failure, but far enough to induce the formation of micro-cracks. The micro-crack thickness measured was close to the thickness measured here (2.20 ± 1.13 μm in (Wolfram et al., 2016), 1.98 ± 0.13 μm in the current study). They found a higher micro-cracks volume fraction (0.09% in (Wolfram et al., 2016), 0.04% in the current study). This can be explained by the mechanical test here being designed to completely fracture the samples: a large part of the micro-cracks were probably absorbed into the main crack. It has been shown that the formation of the main crack may be due to the coalescence of micro-cracks (Zioupos et al., 2008).

Under quasi-static loading, we found that more micro-damage forms in the radius than in the femoral diaphysis and femoral neck, both in terms of total volume fraction and individual volume of the micro-cracks. Considering the energy-dissipating nature of the formation of micro-cracks in the bone tissue, this would mean that more energy is dissipated through micro-crack formation in the radius than the other sites under quasi-static loading. This is consistent with our previous work where we found that the radius is more resistant to crack propagation than the femoral diaphysis and femoral neck under quasi-static loading (Gauthier et al., 2017). A higher volume fraction of micro-cracks, as observed in the radius, results in a higher quantity of energy dissipated and thus a slowdown of the main crack propagation (Ritchie, 1999). The secondary cracks formed under quasi-static loading within the radius present a higher 2ndCr.L3, than in the femoral diaphysis or neck. This characterizes their deviation among bone structural features such as the osteonal boundaries (Fig. 3). More crack deviations may thus occur in the radius than in the femoral diaphysis or femoral neck. It was previously shown that a higher area fraction of osteons resulted in a lower fracture toughness (Mischinski and Ural, 2011) and that the radius and the femur presented a different osteonal system (Gauthier et al., 2018b).

Under fall-like loading, the micro-crack volume fraction and the total volume fracrion (μCr.V/BV and TotCr.V/BV, respectively) in the radius is significantly lower than under quasi-static loading. Similar results were found previously in 2D (Zioupos et al., 2008). This suggests that there is less energy dissipation due to micro-crack formation when cortical bone is loaded under fall-like conditions. Previous results on the effect of loading rate on bone toughness are in accordance with the current result (Gauthier et al., 2017; Kulin et al., 2011; Shannahan et al., 2015; Ural et al., 2011; Zimmermann et al., 2014). Moreover, under fall-like loading, there is no significant difference in crack volume fraction between the different paired anatomical locations. This suggests that, under quasi-static loading, the micro-cracking toughening mechanism is different between the anatomical locations, and more specifically it is more efficient in the radius. Under a higher loading rate, this mechanism dissipates the same energy in the three paired locations. The higher rate thus inhibits a mechanism related to the formation of micro-cracks during a critical loading. These results are consistent with our previous results stating that the radius dissipates more energy under a quasi-static and that there is significantly less dissipated energy under fall-like loading conditions than under quasi-static conditions (Gauthier et al., 2017). In the current study, the loading rate had no significant effect on crack volume fraction for the femoral diaphysis and femoral neck. If micro-cracks seem to be an effective toughening mechanism for the radius, it might therefore not be the only energy dissipating mechanism during crack propagation. Other possible mechanisms might be the difference in micro-structure or in collagen composition between the locations (Gauthier et al., 2018b, 2018a). It is actually assumed that other mechanisms are effective during crack propagation, such as collagen stretching, interfibrillar sliding and crack deflection (Zimmermann and Ritchie, 2015). Also, fatigue damages prior to critical loading has not been considered in the current study whereas it has been shown to have an influence on bone mechanical properties under critical loading (Diab and Vashishth, 2005; Turnbull et al., 2014). The investigation of the effect of such fatigue damages on cortical bone fracture toughness measured under a fall-like loading condition might be of great interest for future studies.

The current study presents some limitations. First, to describe the larger micro-cracks observed after main crack propagation, we defined a new type of crack, called secondary cracks. These features may be associated with the crack branching mechanism that occurs during bone fracture (Turner and Burr, 1993) (Fig. 5). This mechanism has been little studied in the past. Here, we showed that it may have an important role in slowing down crack propagation under quasi-static loading. However, the geometric criteria used here to distinguish the two types of cracks within the volumes were defined empirically and have not been previously considered in the literature. There is no theoretical criterion on their structural features allowing for a distinction between micro-cracks and secondary cracks. Therefore, we chose to also present the total crack volume fraction rather than to separate secondary crack volume fraction and micro-crack volume fraction.

Second, it is possible that the sample preparation protocol might have introduced micro-defects post-hoc. As the aim of this study was to evaluate inter-site differences, and since all the samples were processed with the same protocol, we believe that the comparative investigation is consistent.

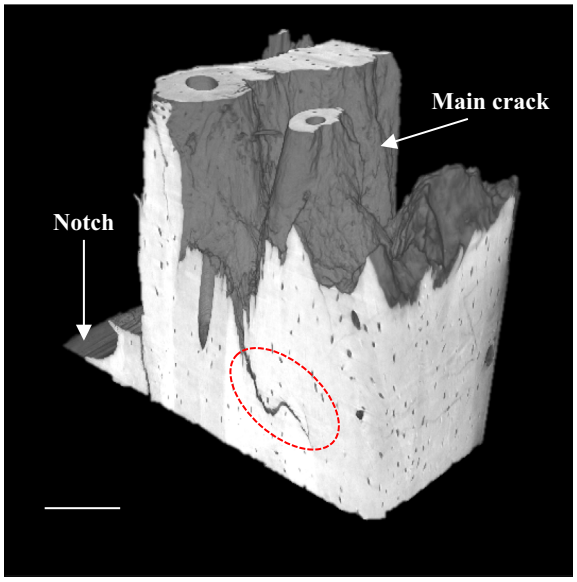

Fig. 5. Volume rendering of radial diaphysis samples under quasi-static loading (woman, 50 y.o.). Note the crack branching mechanisms highlighted by the red label. Scale bar = 500 μm. (For interpretation of the references to colour in this figure legend, the reader is referred to the web version of this article.)

Finally, the population was limited to eight female donors, all of which could be qualified as elderly (50 to 91 y.o.). It is known that the micro-cracking mechanism is age dependent (Zioupos and Currey, 1998). We note, however, that the samples used are representative of a population of postmenopausal women that is more at risk for bone diseases and fall-related traumatic injuries.

To our knowledge, this is the first study analyzing micro-cracks in three dimensions in paired human femoral diaphysis and neck and radial diaphysis. In summary, our results show that micro-cracks play a major role in cortical bone fracture behavior. Analysis on these μCT images can be deepened in order to identify other structural related fracture mechanisms such as crack deflection at the cement line (Koester et al., 2008), or roughness of the fracture surface (Ponson et al., 2013). Future work should consider different fracture mechanisms observed when investigating different anatomical locations (Hernandez and van der Meulen, 2017).

5. Conclusion

In the current study, we investigated the influence of two loading conditions on the morphology of micro-cracks formed during critical loading on eight paired femoral diaphyses, femoral necks and radial diaphyses. The results indicate that both under quasi-static and fall-like loading conditions, a significant amount of micro-cracks and secondary cracks was formed during the fracture process. However, a significant difference in the volume fraction of micro-cracks and secondary cracks induced by the two loading conditions were observed in the radial diaphyses, but not for the femoral diaphysis or neck. Under fall-like loading conditions, micro-cracking is similar for the three paired anatomical locations that were studied. This suggests that while the micro-cracking mechanisms are a major determinant for bone fracture behavior under a quasi-static loading, other parameters have to be investigated to characterize bone crack propagation mechanisms under a fall-like loading. This knowledge would be useful for modeling bone fracture in these three anatomical locations.

Conflict of interest

The authors declare no conflict of interest. The founding sponsors had no role in the design of the study; in the collection, analyses, or interpretation of data; in the writing of the manuscript, and in the decision to publish the results.

Acknowledgments

The authors acknowledge the ESRF ID19 staff for its support for synchrotron data acquisition during the experiment MD923. This work was supported by the LabEx PRIMES (ANR-11-LABX-0063) within the program "Investissements d'Avenir" (ANR-11-IDEX-0007). This study was also partly funded by the Région Auvergne-Rhône-Alpes (14-011125-01) and by the ANR project MUTLIPS (ANR-13-BS09-0006). The authors also want to thank the Fédération INGE'LYSE for its financial support. The work was done in the context of the project France Life Imaging ANR-11-INBS-0006.

Appendix A. Supplementary material

Supplementary data to this article can be found online at https://doi.org/10.1016/j.jbiomech.2019.01.008.

References

Bonewald, L.F., 2011. The amazing osteocyte. J. Bone Miner. Res. 26, 229–238. https://doi.org/10.1002/jbmr.320.

Bonewald, L.F., Johnson, M.L., 2008. Osteocytes, mechanosensing and Wnt signaling. Bone 42, 606–615. https://doi.org/10.1016/j.bone.2007.12.224.

Burr, D.B., Martin, R.B., Schaffler, M.B., Radin, E.L., 1985. Bone remodeling in response to in vivo fatigue microdamage. J. Biomech. 18, 189–200. https://doi.org/10.1016/0021-9290(85)90204-0.

Court-Brown, C.M., Caesar, B., 2006. Epidemiology of adult fractures: A review. Injury 37, 691–697. https://doi.org/10.1016/j.injury.2006.04.130.

Danova, N.A., Colopy, S.A., Radtke, C.L., Kalscheur, V.L., Markel, M.D., Vanderby, R., McCabe, R.P., Escarcega, A.J., Muir, P., 2003. Degradation of bone structural properties by accumulation and coalescence of microcracks. Bone 33, 197–205. https://doi.org/10.1016/S8756-3282(03)00155-8.

Diab, T., Condon, K.W., Burr, D.B., Vashishth, D., 2006. Age-related change in the damage morphology of human cortical bone and its role in bone fragility. Bone 38, 427–431. https://doi.org/10.1016/j.bone.2005.09.002.

Diab, T., Vashishth, D., 2005. Effects of damage morphology on cortical bone fragility. Bone 37, 96–102. https://doi.org/10.1016/j.bone.2005.03.014.

Dong, P., Haupert, S., Hesse, B., Langer, M., Gouttenoire, P.J., Bousson, V., Peyrin, F., 2014. 3D osteocyte lacunar morphometric properties and distributions in human femoral cortical bone using synchrotron radiation micro-CT images. Bone 60, 172–185. https://doi.org/10.1016/j.bone.2013.12.008.

Foldhazy, Z., 2005. Exercise-induced strain and strain rate in the distal radius. J. Bone Jt. Surg. - Br. 87–B, 261–266. https://doi.org/10.1302/0301-620X.87B2.14857.

Follet, H., Viguet-Carrin, S., Burt-Pichat, B., Dépalle, B., Bala, Y., Gineyts, E., Munoz, F., Arlot, M., Boivin, G., Chapurlat, R.D., Delmas, P.D., Bouxsein, M.L., 2011. Effects of preexisting microdamage, collagen cross-links, degree of mineralization, age, and architecture on compressive mechanical properties of elderly human vertebral trabecular bone. J. Orthop. Res. 29, 481–488. https://doi.org/10.1002/jor.21275.

Gauthier, R., Follet, H., Langer, M., Gineyts, E., Rongiéras, F., Peyrin, F., Mitton, D., 2018a. Relationships between human cortical bone toughness and collagen cross-links on paired anatomical locations. Bone 112, 202–211. https://doi.org/10.1016/j.bone.2018.04.024.

Gauthier, R., Follet, H., Langer, M., Meille, S., Chevalier, J., Rongiéras, F., Peyrin, F., Mitton, D., 2017. Strain rate influence on human cortical bone toughness: A comparative study of four paired anatomical sites. J. Mech. Behav. Biomed. Mater. 71, 223–230. https://doi.org/10.1016/j.jmbbm.2017.03.015.

Gauthier, R., Langer, M., Follet, H., Olivier, C., Gouttenoire, P.-J., Helfen, L., Rongiéras, F., Mitton, D., Peyrin, F., 2018b. 3D micro structural analysis of human cortical bone in paired femoral diaphysis, femoral neck and radial diaphysis. J. Struct. Biol. 204, 182–190. https://doi.org/10.1016/j.jsb.2018.08.006.

Graham, J.M., Ayati, B.P., Holstein, S.A., Martin, J.A., 2013. The role of osteocytes in targeted bone remodeling: a mathematical model. PLoS One 8, 10–14. https://doi.org/10.1371/journal.pone.0063884.

Granke, M., Makowski, A.J., Uppuganti, S., Nyman, J.S., 2016. Prevalent role of porosity and osteonal area over mineralization heterogeneity in the fracture toughness of human cortical bone. J. Biomech. 49, 2748–2755. https://doi.org/10.1016/j.jbiomech.2016.06.009.

Griffith, A.A., 1921. The phenomena of rupture and flow in solids. Philos. Trans. R. Soc. A Math. Phys. Eng. Sci. 221, 163–198. https://doi.org/10.1098/rsta.1921.0006.

Gupta, H.S., Krauss, S., Kerschnitzki, M., Karunaratne, A., Dunlop, J.W.C., Barber, A.H., Boesecke, P., Funari, S.S., Fratzl, P., 2013. Intrafibrillar plasticity through mineral/collagen sliding is the dominant mechanism for the extreme toughness of antler bone. J. Mech. Behav. Biomed. Mater. 28, 366–382. https://doi.org/10.1016/j.jmbbm.2013.03.020.

Haupert, S., Guérard, S., Mitton, D., Peyrin, F., Laugier, P., 2015. Quantification of nonlinear elasticity for the evaluation of submillimeter crack length in cortical bone. J. Mech. Behav. Biomed. Mater. 48, 210–219. https://doi.org/10.1016/j.jmbbm.2015.04.013.

Hernandez, C.J., van der Meulen, M.C., 2017. Understanding bone strength is not enough. J. Bone Miner. Res. 32, 1157–1162. https://doi.org/10.1002/jbmr.3078.

Katsamenis, O.L., Jenkins, T., Quinci, F., Michopoulou, S., Sinclair, I., Thurner, P.J., 2013. A novel videography method for generating crack-extension resistance curves in small bone samples. PLoS One 8, e55641. https://doi.org/10.1371/journal.pone.0055641.

Koester, K.J., Ager, J.W., Ritchie, R.O., 2008. The true toughness of human cortical bone measured with realistically short cracks. Nat. Mater. 7, 672–677. https://doi.org/10.1557/mrs2008.195.

Kulin, R.M., Jiang, F., Vecchio, K.S., 2011. Effects of age and loading rate on equine cortical bone failure. J. Mech. Behav. Biomed. Mater. 4, 57–75. https://doi.org/10.1016/j.jmbbm.2010.09.006.

Larrue, A., Rattner, A., Peter, Z.A., Olivier, C., Laroche, N., Vico, L., Peyrin, F., 2011. Synchrotron radiation micro-CT at the Micrometer scale for the analysis of the three-dimensional morphology of microcracks in human trabecular bone. PLoS One 6, e21297. https://doi.org/10.1371/journal.pone.0021297.

Marotti, G., 1979. Osteocyte orientation in human lamellar bone and its relevance to the morphometry of periosteocytic lacunae. Metab. Bone Dis. Relat. Res. 1, 325–333. https://doi.org/10.1016/0221-8747(79)90027-4.

Martín-Badosa, E., Elmoutaouakkil, A., Nuzzo, S., Amblard, D., Vico, L., Peyrin, F., 2003. A method for the automatic characterization of bone architecture in 3D mice microtomographic images. Comput. Med. Imaging Graph. 27, 447–458. https://doi.org/10.1016/S0895-6111(03)00031-4.

Mischinski, S., Ural, A., 2011. Interaction of microstructure and microcrack growth in cortical bone: a finite element study. Comput. Methods Biomech. Biomed. Engin., 1–14 https://doi.org/10.1080/10255842.2011.607444.

Mohsin, S., O'Brien, F.J., Lee, T.C., 2006. Microcracks in compact bone: A three-dimensional view. J. Anat. 209, 119–124. https://doi.org/10.1111/j.1469-7580.2006.00554.x.

Nalla, R.K., Kruzic, J.J., Ritchie, R.O., 2004. On the origin of the toughness of mineralized tissue: Microcracking or crack bridging? Bone 34, 790–798. https://doi.org/10.1016/j.bone.2004.02.001.

Norman, T.L., Wang, Z., 1997. Microdamage of human cortical bone: Incidence and morphology in long bones. Bone 20, 375–379. https://doi.org/10.1016/S8756-3282(97)00004-5.

O'Brien, F.J., Taylor, D., Dickson, G.R., Lee, T.C., 2000. Visualisation of three-dimensional microcracks in compact bone. J. Anat. 197 Pt 3, 413–420. https://doi.org/10.1046/j.1469-7580.2000.19730413.x.

Paganin, D., Mayo, S.C., Gureyev, T.E., Miller, P.R., Wilkins, S.W., 2002. Simultaneous phase and amplitude extraction from a single defocused image of a homogeneous object. J. Microsc. 206, 33–40. https://doi.org/10.1046/j.1365-2818.2002.01010.x.

Ponson, L., Srivastava, A., Osovski, S., Bouchaud, E., Tvergaard, V., Needleman, A., 2013. Correlating toughness and roughness in ductile fracture 1–5.

Poundarik, A.A., Diab, T., Sroga, G.E., Ural, A., Boskey, A.L., Gundberg, C.M., Vashishth, D., 2012. Dilatational band formation in bone. Proc. Natl. Acad. Sci. U. S. A. 109, 19178–19183. https://doi.org/10.1073/pnas.1201513109.

Poundarik, A.A., Vashishth, D., 2015. Multiscale imaging of bone microdamage. Connect. Tissue Res. 56, 87–98. https://doi.org/10.3109/03008207.2015.1008133.

Ritchie, R.O., 1999. Mechanisms of fatigue-crack propagation in ductile and brittle solids. Int. J. Fract. 100, 55–83. https://doi.org/10.1023/A:1018655917051.

Ritchie, R.O., 1988. Mechanisms of fatigue crack propagation in metals, ceramics and composites: Role of crack tip shielding. Mater. Sci. Eng. A 103, 15–28. https://doi.org/10.1016/0025-5416(88)90547-2.

Schaffler, M.B., Choi, K., Milgrom, C., 1995. Aging and matrix microdamage accumulation in human compact bone. Bone 17, 521–525. https://doi.org/10.1016/8756-3282(95)00370-3.

Schladitz, K., Ohser, J., Nagel, W., 2006. Measuring intrinsic volumes in digital 3d images. Discret. Geom. Comput. Imag. 4245, 247–258. https://doi.org/10.1007/11907350_21.

Seeman, E., Delmas, P.D., 2006. Bone quality–the material and structural basis of bone strength and fragility. N. Engl. J. Med. 354, 2250–2261. https://doi.org/10.1056/NEJMra053077.

Shannahan, L., Weerasooriya, T., Gunnarsson, A., Sanborn, B., Lamberson, L., Shannahan, L., Lamberson, L., Weerasooriya, T., Gunnarsson, A., 2015. Rate-dependent fracture modes in human femoral cortical bone. Int. J. Fract. 194, 81–92. https://doi.org/10.1007/s10704-015-0035-0.

Steiner, J.A., Ferguson, S.J., van Lenthe, G.H., 2016. Screw insertion in trabecular bone causes peri-implant bone damage. Med. Eng. Phys. 38, 417–422. https://doi.org/10.1016/j.medengphy.2016.01.006.

Tang, S.Y., Vashishth, D., 2010. Non-enzymatic glycation alters microdamage formation in human cancellous bone. Bone 46, 148–154. https://doi.org/10.1016/j.bone.2009.09.003.

Tang, S.Y., Vashishth, D., 2007. A non-invasive in vitro technique for the three-dimensional quantification of microdamage in trabecular bone. Bone 40, 1259–1264. https://doi.org/10.1016/j.bone.2006.10.031.

Tang, S.Y., Zeenath, U., Vashishth, D., 2007. Effects of non-enzymatic glycation on cancellous bone fragility. Bone 40, 1144–1151. https://doi.org/10.1016/j.bone.2006.12.056.

The American Society of Mechanical Engineers (ASME), 2006. E 1820-01: Standard Test Method for Measurement of Fracture Toughness. . . . . Philadelphia PA Am. Soc. Test. . . . 46.

Turnbull, T.L., Baumann, A.P., Roeder, R.K., 2014. Fatigue microcracks that initiate fracture are located near elevated intracortical porosity but not elevated mineralization. J. Biomech. 47, 3135–3142. https://doi.org/10.1016/j.jbiomech.2014.06.022.

Turner, C.H., Burr, D.B., 1993. Basic biomechanical measurements of bone: a tutorial. Bone 14, 595–608. https://doi.org/10.1016/8756-3282(93)90081-K.

Ural, A., Zioupos, P., Buchanan, D., Vashishth, D., 2011. The effect of strain rate on fracture toughness of human cortical bone: A finite element study. J. Mech. Behav. Biomed. Mater. 4, 1021–1032. https://doi.org/10.1016/j.jmbbm.2011.03.011.

Vashishth, D., 2007. The role of the collagen matrix in skeletal fragility. Curr. Osteoporos. Rep. 5, 62–66. https://doi.org/10.1007/s11914-007-0004-2.

Vashishth, D., Behiri, J.C., Bonfield, W., 1997. Crack growth resistance in cortical bone: Concept of microcrack toughening. J. Biomech. 30, 763–769. https://doi.org/10.1016/S0021-9290(97)00029-8.

Vashishth, D., Koontz, J., Qiu, S.J., Lundin-Cannon, D., Yeni, Y.N., Schaffler, M.B., Fyhrie, D.P., 2000. In vivo diffuse damage in human vertebral trabecular bone. Bone 26, 147–152. https://doi.org/10.1016/S8756-3282(99)00253-7.

Voide, R., Schneider, P., Stauber, M., Wyss, P., Stampanoni, M., Sennhauser, U., Van Lenthe, G.H., Müller, R., 2009. Time-lapsed assessment of microcrack initiation and propagation in murine cortical bone at submicrometer resolution. Bone 45, 164–173. https://doi.org/10.1016/j.bone.2009.04.248.

Wang, X., Masse, D.B., Leng, H., Hess, K.P., Ross, R.D., Roeder, R.K., Niebur, G.L., 2007. Detection of trabecular bone microdamage by micro-computed tomography. J. Biomech. 40, 3397–3403. https://doi.org/10.1016/j.jbiomech.2007.05.009.

Wolfram, U., Schwiedrzik, J.J., Mirzaali, M.J., Bürki, A., Varga, P., Olivier, C., Peyrin, F., Zysset, P.K., 2016. Characterizing microcrack orientation distribution functions in osteonal bone samples. J. Microsc. 00, 1–14. https://doi.org/10.1111/jmi.12440.

Zarrinkalam, K., Kuliwaba, J., Martin, R., Wallwork, M., Fazzalari, N., 2005. New insights into the propagation of fatigue damage in cortical bone using confocal microscopy and chelating fluorochromes. Eur. J. Morphol. 42, 81–90. https://doi.org/10.1080/09243860500096206.

Zimmermann, E.A., Gludovatz, B., Schaible, E., Busse, B., Ritchie, R.O., 2014. Fracture resistance of human cortical bone across multiple length-scales at physiological strain rates. Biomaterials 35, 5472–5481. https://doi.org/10.1016/j.biomaterials.2014.03.066.

Zimmermann, E.A., Ritchie, R.O., 2015. Bone as a structural material. Adv. Healthc. Mater. 4, 1287–1304. https://doi.org/10.1002/adhm.201500070.

Zioupos, P., Currey, J.D., 1998. Changes in the stiffness, strength, and toughness of human cortical bone with age. Bone 22, 57–66. https://doi.org/10.1016/S8756-3282(97)00228-7.

Zioupos, P., Hansen, U., Currey, J.D., 2008. Microcracking damage and the fracture process in relation to strain rate in human cortical bone tensile failure. J. Biomech. 41, 2932–2939. https://doi.org/10.1016/j.jbiomech.2008.07.025.